Frequency selective heterojunction metal-insulator-metal mirror for surface plasmons

Yongsop Hwang (황용섭),[*] Jonghwa Shin (신종화), Jae-Eun Kim (김재은), and Hae Yong Park (박해용)
Department of Physics, KAIST, Daejeon 305-701, Korea

Chul-Sik Kee (기철식)[†]
Nanophotonics Laboratory, Advanced Photonics Research Institute, GIST, Gwangju 500-712,
and Center for Subwavelength Optics, Korea

The authors introduce a mode-gap mirror for surface plasmon polaritons in a metal-insulator-metal (MIM) structure. At the heterojunction of MIMs which consists of two MIMs of different insulators, it is shown that a mode gap exists for a certain frequency range and the junction works as an effective mirror. Transmission and reflection properties of plasmonic modes at the interface of the heterojunction are investigated, and explained by the band theory. By showing that the mirror has high reflection and transmission of nearly zero, it is verified that the frequency range in which no plasmonic modes exist is an actual mode-gap range. It is also shown that by varying both the thickness and the dielectric constant of the insulator layer, one can select the frequency range in which the reflection coefficient is greater than 0.9.

I. INTRODUCTION

Surface plasmon polaritons (SPPs) have been investigated by many researchers because of the possibility of miniaturizing photonic devices to subwavelength scale.[1] To reduce the size of photonic devices, confining light in a small structure is important. Since the metal-insulator-metal (MIM) structure is one of the effective ways to control the size of SPP modes, its physical properties such as dispersion relations and field distributions have been investigated both theoretically[2–6] and experimentally.[7,8] Heterostructures of MIMs which have different metals for the upper and lower claddings were also studied in detail.[9] MIM structures are widely applied to photonic devices such as waveguides,[10–12] bends and splitters,[13] filters,[14,15] negative refraction lenses,[16] lasers,[17] and so on.

As a mirror is one of the very basic and important devices in photonic circuits, there have been some reports on MIM mirrors. However, most of them are designed in the scheme of a Bragg reflector,[18–20] so that they must have periodic structures which require considerable effort to fabricate. For this reason we introduce a mode-gap mirror which is designed as a junction of two MIMs, each with an insulator layer of different dielectric constant, a heterojunction MIM mirror.

In Sec. II, the design of the two-dimensional heterojunction MIM mirror is presented and the calculation methods used are described. In Sec. III, the existence of a mode gap in the heterojunction MIM mirror is addressed. The dispersion relation of each MIM is investigated and the frequency ranges are categorized according to their expected transmission and reflection properties. In Sec. IV, the transmission and reflection spectra obtained by numerical calculations are shown and the results are explained. The E-field and H-field profiles for selected frequencies are also shown. In Sec. V, the reflection property of the MIM mirror is investigated for various thicknesses and dielectric constants of insulators. Finally, in Sec. VI we conclude the paper by summarizing the properties and advantages of the heterojunction MIM mirror, and suggesting its possibilities of applications.

II. DESIGN AND METHOD

We designed the SPP mirror in an MIM structure by introducing an electric permittivity difference between the two different sandwiched insulators, as depicted in Fig. 1. The material of the first part where the light is incident is air, and that of the second part is a dielectric of $\epsilon_d = 12$. The metal which covers the insulator layer is silver and its optical properties are characterized by the Drude model:

$$\epsilon_m(\omega)/\epsilon_f = 1 - \frac{\omega_p^2}{\omega^2 + 2i\omega\delta}, \qquad (1)$$

where ϵ_f is a fitting permittivity in the visible range, ω_p the bulk plasma frequency, and δ the damping constant. $\epsilon_f = 6.8$, $\omega_p = 3.8$ eV, and $\delta = 0.02$ eV are used as in Ref. 21 to fit the optical constants of silver in the optical frequency range which was reported by Johnson and Christy.[22] The thickness d of the insulator layers of two MIMs is 26.6 nm in most of the discussion except for in Sec. V. The SPPs would be reflected at the interface of the air and the dielectric layer, so that the system may function as a frequency selective mirror. This design is applicable for most of the SPP modes of the optical frequency range.

For the simulations, we used a freely available software package with subpixel smoothing for increased accuracy,[23] the finite-difference time-domain (FDTD) method,[24] to obtain the band diagram and the transmission and reflection coefficients of the SPP modes. To obtain the diagram, we employed the periodic boundary conditions and for the transmission and reflection, the perfectly matched layer is used. The periodic boundary conditions are employed in the y direction to avoid the undesirable instability which may occur when the metal is overlapped by a perfectly matched layer,[25,26] and the silver layers are set to be thick enough for the periodic structure to be considered as a single MIM structure. A time Fourier transform at all space points of our FDTD results is taken in order to define R and T. The field profiles are obtained by launching a continuous wave source at the same position.
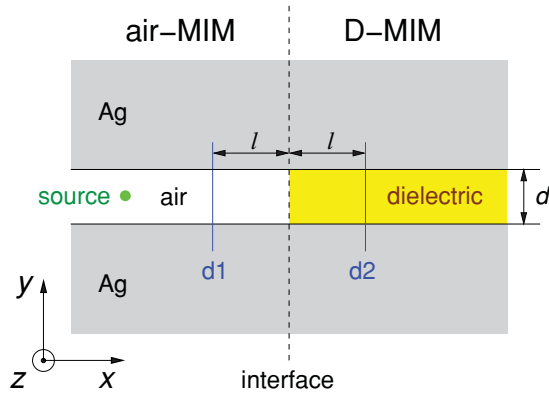
FIG. 1. (Color online) Design of a heterojunction MIM mirror for SPPs. It consists of two MIM structures, an air-MIM and a D-MIM, which have air and a dielectric as their insulator layers, respectively. Silver is used for metal claddings. The H-field source which is polarized in the z direction is launched into the air-MIM. The detectors d1 and d2 are located at the same distance from the interface of the two MIMs.

III. EXISTENCE OF MODE GAP

To investigate the reflection mechanism of SPP modes in the heterojunction MIM structure, we obtained the dispersion relation of each MIM structure separately and classified the frequency ranges by the mode-matching characteristics as listed in Table I. Figure 2(a) shows the dispersion relations of SPPs in the air-MIM structure where the insulator between metals is air, and Fig. 2(b) those in the D-MIM where the insulator is the dielectric with $\epsilon_d = 12$. The dispersion relations are shown for the real values of frequencies ω and propagation vectors Re(β). The real values of frequencies as functions of the imaginary values of propagation vectors Im(β) are not shown as our main concerns in this study are the transmission and the reflection properties at the interface between the air-MIM and the D-MIM. Three frequency regions are defined according to the dispersion relation of the D-MIM. Regions I, II, and III represent the frequency ranges $\omega < 3.30 \times 10^{15}$ Hz, 3.30×10^{15} Hz $\leqslant \omega < 4.10 \times 10^{15}$ Hz, and 4.10×10^{15} Hz $\leqslant \omega < 5.81 \times 10^{15}$ Hz , respectively. For all the calculations the H field has only a z component. Furthermore within the lowest band, H_z is symmetric about the guiding center of the MIM. For the silver-air-silver (air-MIM) the upper bound frequency for the first band is at $\omega = 5.36 \times 10^{15}$ Hz. For the dielectric with $\epsilon_d = 12$ between the silver layers (D-MIM), however, the first band has the upper bound at $\omega = 3.30 \times 10^{15}$ Hz. These upper bound frequencies are known as SPP resonance frequencies ω_{sp} which can be analytically obtained from the equation $\omega_{sp}/\omega_p = \sqrt{\epsilon_f/(\epsilon_f + \epsilon_d)}$

TABLE I. Classification of the frequency regions according to their mode-matching characteristics.

Region	ω (10^{15} Hz)	Characteristic
I	$0 < \omega < 3.30$	Mode match
II	$3.30 \leqslant \omega < 4.10$	Mode mismatch
III	$4.10 \leqslant \omega < 5.81$	Band gap
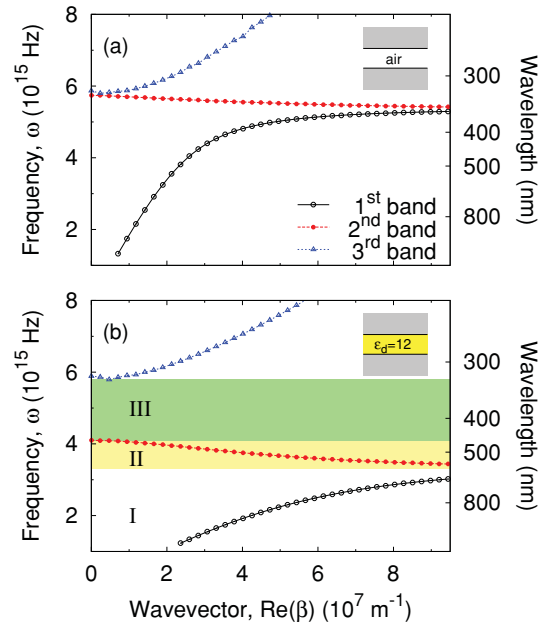
FIG. 2. (Color online) Dispersion relations of electromagnetic fields in the two MIM structures. The insulator is (a) air in the air-MIM and (b) a dielectric of $\epsilon_d = 12$ in the D-MIM. The thickness of the insulator layers $d = 26.6$ nm in both MIM structures. In (b), region I (white) represents the mode-matching frequency range for the heterojunction, region II (yellow) the mode-mismatching range, and region III (green) the band-gap region.

when the damping constant δ is negligible compared to the plasma frequency ω_p, i.e., $2\delta/\hbar\omega_p \ll 1$. The equation gives $\omega_{sp} = 5.39 \times 10^{15}$ Hz and 3.47×10^{15} Hz for the air-MIM and the D-MIM, respectively. The differences between the FDTD simulations and the analytically obtained values are considered as numerical errors.

The SPP modes of the air-MIM in region I can couple to those of the D-MIM in region I for they have the same symmetry. In region II, the second band of the D-MIM, the SPP modes are antisymmetric. Thus, the modes of the air-MIM cannot be coupled to those of the D-MIM in this frequency range due to the mismatch of the mode symmetries. In particular, since the group velocity in this region is negative in the D-MIM, effective reflection is expected for the SPPs in this frequency regime. In region III, the D-MIM has a band gap, so that there is no matching mode between the two MIM structures. Regions II and III together may be called a mode-gap region since no matching mode between the two MIM structures exists here. Therefore, different reflection properties will be exhibited for these three different visible spectral regions; that is, we can make a frequency selective mirror for SPPs utilizing the mode gap of the heterojunction MIM structure. As the dispersion relation of a MIM structure is a function of the electric permittivity and the thickness of the insulator layer,[2] the range of a mode gap can be controlled by using materials of different ϵ_d and by varying its thickness d.

Even though the origin of the mode gap can be understood, still a question remains as to whether the mode gap is valid for all values of wave vectors, because there is no zone folding caused by any periodic structures, as the MIM structure is not periodic. If there is a certain upper frequency limit for the first

band above which no mode can have a higher frequency, then the frequency range of region I is determined. And if there is a cutoff frequency for the third band below which no mode can have a lower frequency, then it determines the upper bound of the frequency range of region III. As there have been reports on the asymptotic behavior of the first band of an MIM and the existence of a cutoff frequency in the third band by both analytic[2] and numerical[12] analyses, the mode gap exists for all values of wave vectors in the present MIM structure. In the next section, the validity of the existence of the mode gap in this heterojunction MIM structure is shown from the transmission and reflection properties.

IV. TRANSMISSION AND REFLECTION

In order to investigate the performance of the heterojunction of the MIM as a mirror, the transmission and reflection coefficients are calculated by using the two-dimensional FDTD method and the results are depicted in Fig. 3. We launched a z-polarized H-field line source along the z axis into the insulator layer. Two detectors d1 and d2 are positioned as in Fig. 1 for the measurement of the power flux, d1 in the air-MIM and d2 in the D-MIM. Both are located at the same distance l from the interface.

First, from the fluxes measured with the two detectors, we obtained the transmission $T_{tot} = \Phi_{d2}/\Phi_{0,d1}$ and the reflection $R_{tot} = -\Phi_{d1}/\Phi_{0,d1}$, where $\Phi_{0,d1}$ is the flux measured with d1 for an Air-MIM waveguide only, Φ_{d1} the flux of the reflected wave measured with d1 for the heterojunction MIM mirror, and Φ_{d2} the flux measured with d2 for the heterojunction MIM mirror. The electromagnetic fields used to calculate Φ_{d1} are found by subtraction of those from two separate FDTD calculations, one with the air/dielectric interface and the other without. To obtain the transmission and the reflection coefficients T and R at the interface of the MIM mirror, the propagation losses are deducted from the total loss to eliminate

the propagation losses. First, we calculated the transmissions $T_{air}(l)$ and $T_D(l)$ for the propagation of the distance l which is half of the distance between the two detectors d1 and d2 in the air-MIM and in the D-MIM waveguides, respectively. Then we used the following relationships to get T and R:

$$T = \frac{T_{tot}}{T_{air}(l)T_D(l)}, \quad R = \frac{R_{tot}}{T_{air}(2l)}. \quad (2)$$

For the calculation of the transmission T, the total transmission T_{tot} is divided by the product of $T_{air}(l)$ and $T_D(l)$, since the fields propagate the distance l in the air-MIM and additional l in the D-MIM. This way of loss elimination is possible because the fields decay exponentially with the propagation length in the MIM waveguides. For the calculation of the reflection R, since the fields propagate the distance $2l$ in the air-MIM, we divided the total reflection R_{tot} by $T_{air}(2l)$.

As expected from the analysis of the dispersion relations in Sec. III, Fig. 3 shows that the transmission T ($\simeq 0.7$) is higher than the reflection R ($\simeq 0.3$) in most of the mode-matching range, region I. In region II, the transmission T is nearly zero and the reflection R increases as the frequency increases and becomes greater than 0.9. It is evidence supporting the idea that the mode mismatching causes high reflection at the interface. In region III, the transmission $T \simeq 0$, but the reflection R decreases as the frequency increases. Here it is verified that regions II and III are an actual mode gap by showing that the transmission $T \simeq 0$, in which no SPP modes of the corresponding frequency range from the air-MIM are allowed inside the D-MIM.

Figure 4 displays the field profiles of the SPP modes, each at a representative frequency in region I and II. The field profiles in region I are depicted for $\omega = 2.48 \times 10^{15}$ Hz in Fig. 4(a). Since the E_x field is confined at the surface between the metal and the insulator, this mode is a surface plasmon mode. The fields propagate beyond the interface of the heterojunction, because there exist matching modes between the air-MIM and the D-MIM. In Fig. 4(b), it is observed that the SPP fields of frequency $\omega = 3.83 \times 10^{15}$ Hz in region II are mostly reflected at the interface and no field is transmitted. Field profiles in region III are similar to those in region II.

V. VARIATION OF THICKNESS AND REFRACTIVE INDEX

The main design parameters of the proposed heterojunction MIM mirror are the thickness of the insulator layer and the refractive index of the dielectric in the D-MIM. Therefore the effect of the thickness and the refractive index of the insulator layer on the reflection is studied. Figure 5(a) shows that the frequency range of high reflection where the reflection $R > 0.9$ becomes narrower as the thickness d of the insulator increases. We can see that the lower bound frequency ω_l of the high R region does not change much with the thickness d, but its upper bound frequency ω_h decreases as d increases. More specifically, ω_h is nearly constant at $\omega_h = 4.46 \times 10^{15}$ Hz in the range of $d < 75$ nm, while it decreases as d increases above 75 nm. The dielectric constant ϵ_d in the D-MIM is varied with a fixed thickness of insulator layer at $d = 26.6$ nm and the reflection R is calculated and plotted in Fig. 5(b). It shows that the width of the frequency range of high R becomes larger as the dielectric constant ϵ_d increases. Differently from the
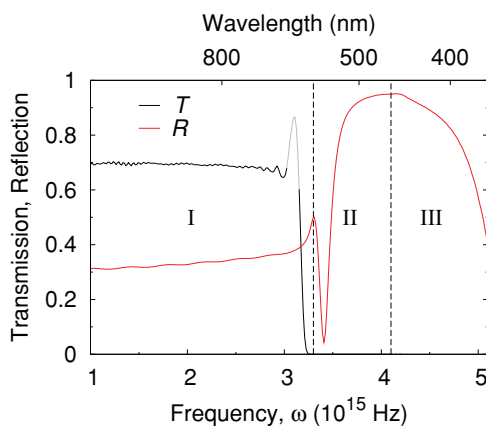
FIG. 3. (Color online) Transmission and reflection spectra of SPP modes at the interface in a heterojunction MIM structure as functions of frequency. In region I, $T \simeq 0.7$ and $R \simeq 0.3$ for most of the frequencies. In regions II and III, the mode-gap region, $T \simeq 0$. $R > 0.9$ for the frequencies larger than $\omega = 3.70 \times 10^{15}$ Hz in region II, and gradually decreases as the frequency increases in region III. The peak in the transmission spectrum colored with gray is considered to be caused by a numerical error.

(a)

(b)
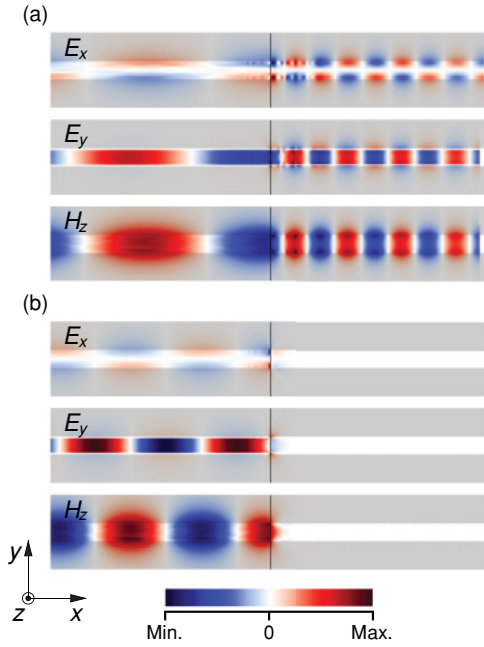
FIG. 4. (Color online) Field profiles of E_x, E_y, and H_z. (a) In region I, the mode-matching region, for $\omega = 2.48 \times 10^{15}$ Hz. (b) In region II, the mode-gap region, for $\omega = 3.83 \times 10^{15}$ Hz. The fields in region I are transmitted beyond the interface, but those in region II are reflected at the interface. Field profiles in region III are omitted as they are similar to those in region II.

thickness variation, we can see that ω_h of the high R region is almost constant, but the lower bound frequency ω_l decreases as ϵ_d increases. Therefore, the central frequency value and the width of the frequency range of high reflection can be chosen in the frequency interval 3.70×10^{15} Hz $< \omega < 4.46 \times 10^{15}$ Hz by the variation of the thickness and dielectric constant of the insulator layer.

To understand the relation between the reflection R and the thickness of the insulator layer, for three different thicknesses $d = 26.6, 79.8$, and 133.0 nm, depicted are the dispersion relations of the first band of the air-MIM in Fig. 6(a) and those of the first and the third bands of the D-MIM in Fig. 6(b). The dielectric constant of the D-MIM is fixed at $\epsilon_d = 12$ in Fig. 6(b). The second bands are not depicted since the mode gaps are determined by the frequency edges of the first and the third bands. In Fig. 6(a), as the propagation wave vector increases, the frequency of SPPs increases and approaches the surface plasmon frequency. The value of asymptotic frequency ω_a of the air-MIM does not change as the thickness of the air layer changes; therefore the frequency range of SPPs of the first bands are the same for all three thicknesses. As can be seen in Fig. 6(b) the main difference in the dispersion relations among the MIM structures of different insulator thicknesses is the value of the cutoff frequencies ω_c of the third bands of the D-MIMs; the thicker the D-MIM, the lower the cutoff frequency.

Since the values of ω_a of the first bands of the D-MIMs are the same at $\omega_a = 3.0 \times 10^{15}$ Hz for different insulator thicknesses, the lower bound ω_l of the frequency range of high R in Fig. 5(a) is not affected by the thickness variation of the insulator layers. Also the decrement of the upper bound

(a)

(b)
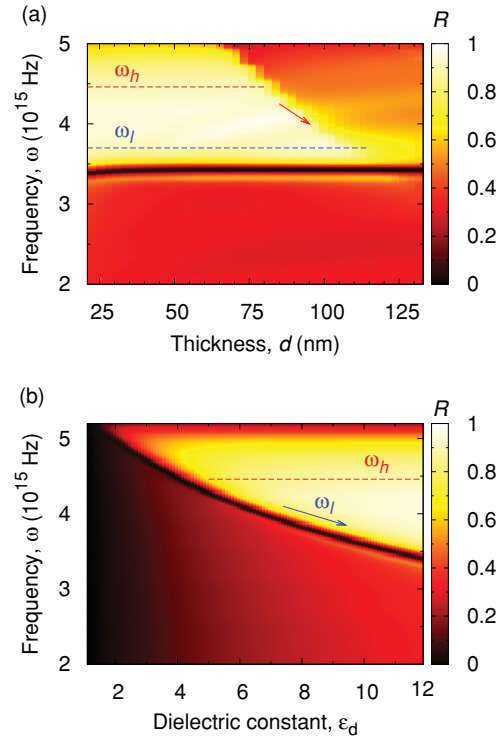
FIG. 5. (Color online) Reflection coefficient R for various thicknesses d and dielectric constants ϵ_d of the insulator layer. (a) The dielectric constant is fixed at $\epsilon_d = 12$ while the thickness of insulator d varies. The lower bound frequency ω_l of the high reflection range where $R > 0.9$ is almost constant at $\omega = 3.70 \times 10^{15}$ Hz, and also there is the upper bound frequency ω_h at $\omega = 4.46 \times 10^{15}$ Hz for $d < 75$ nm, but ω_h decreases as d increases for $d > 75$ nm. (b) The thickness of insulator is fixed at $d = 26.6$ nm while ϵ_d varies. The upper bound frequency ω_h of the high reflection range where $R > 0.9$ is about $\omega = 4.46 \times 10^{15}$ Hz, while its lower bound decreases as ϵ_d increases. In both (a) and (b), the black lines drawn just below the lower bound frequencies ω_l which represent the nearly zero reflection are in the frequency range of very low group velocity of SPP modes, where the SPP fields do not actually propagate.

frequency ω_h of the high R region with increasing d for $d > 80$ nm is due to the decrement of the cutoff frequency ω_c of the third bands of the D-MIM with increasing d [see Fig. 6(b)].

This dependence of ω_c on the insulator thickness is explained with the orders of SPP modes. The third band of the thinnest D-MIM of $d = 26.6$ nm is of bulk plasmon modes which have the electromagnetic fields spread in both the metal and the insulator layers. However, the third bands of the D-MIM of $d = 79.8$ nm and 133.0 nm are not of bulk plasmon modes. They are of the third-order modes whose H_z fields are symmetric about the guiding center and have the antinodes at the center of the insulator layer, and thus the modes in the first band of the air-MIM may couple to them. But their coupling efficiency is not so good that the reflection may not be negligible. This can be observed in Fig. 5(a). The reflection does not suddenly become zero for the frequencies $\omega > \omega_c$ in the thickness range $d > 80$ nm.

To study the dependence of the reflection coefficient R on the dielectric constant ϵ_d of the insulator layer of D-MIM, the dispersion relations of the D-MIMs for three different
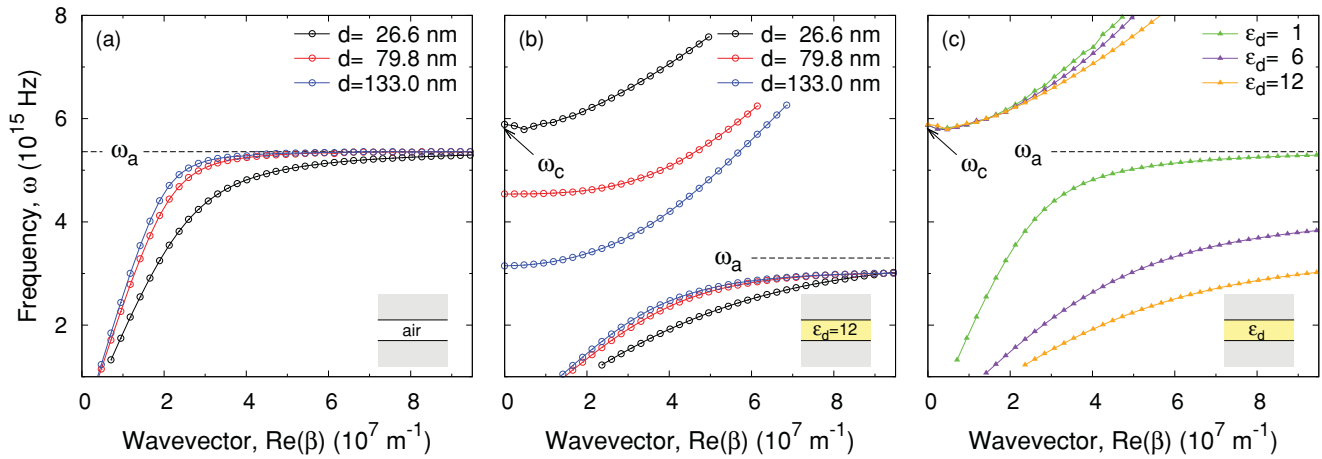
FIG. 6. (Color online) Dispersion relations of the first and the third bands of electromagnetic fields in the MIM structures for different thicknesses and dielectric constants of insulator layers. (a) Dispersion relations of the air-MIMs for the air thicknesses $d = 26.6, 79.8$, and 133.0 nm. Asymptotic frequencies of the first bands are the same at $\omega_a = 5.36 \times 10^{15}$ Hz for different thicknesses. (b) Dispersion relations of the D-MIMs with $\epsilon_d = 12$ for the dielectric thicknesses $d = 26.6, 79.8$, and 133.0 nm. Asymptotic frequencies of the first bands are the same at $\omega_a = 3.30 \times 10^{15}$ Hz for different thicknesses. The cutoff frequency ω_c of the third band decreases as the thickness gets thicker, that is, the frequency width of the mode-gap range becomes narrower and the center frequency of the mode gap decreases. (c) Dispersion relations of the D-MIMs with the thickness $d = 26.6$ nm for the dielectric constants $\epsilon_d = 1, 6$, and 12. Asymptotic frequency ω_a of the first bands decreases as ϵ_d increases, while the cutoff frequencies ω_c are the same for different dielectric constants. Therefore, the frequency width of the mode-gap range becomes wider and the center frequency of the mode gap decreases as the dielectric constant increases.

dielectric constants, $\epsilon_d = 1, 6$, and 12, with the same insulator thickness $d = 26.6$ nm are depicted in Fig. 6(c). The relevant bands of concern are the first and the third bands because the mode gap, the regions II and III, is between the highest frequency ω_a of the first band and the lowest ω_c of the third band. The frequency range of the first band is shifted to lower frequencies for larger ϵ_d, while the cutoff frequency ω_c of the third band does not change with ϵ_d variation in this thin enough MIM structure. This phenomenon may have its origin in the fact that most parts of the SPP waves in the first and second bands locate in the insulator layer and the modes at a certain wave vector may have lower frequencies in the D-MIM of larger ϵ_d just as in the conventional dielectric stripe waveguides. Thus the frequency range of high R can be controlled by varying the value of ϵ_d for the D-MIM structure which changes the lower bound frequency of the mode-gap region.

VI. CONCLUSION

In conclusion, a compact and frequency selective mirror for SPPs in a heterojunction MIM structure is designed and its reflection property is investigated. The MIM mirror reflects SPPs with the transmission coefficient nearly zero for frequencies in the mode-gap region. The existence of a mode-gap is predicted by investigating the dispersion relations and proved by showing the transmission and reflection properties of SPPs in the MIM mirror. The mode gap is shown to exist between the asymptotic frequency of the first band and the cutoff frequency of the third band. This mirror shows a reflection coefficient at the interface larger than 0.9 for a frequency range in the mode mismatch region so that it can be used as a frequency selective mirror. Also the dependence of the reflection coefficient on the thickness and the dielectric constant of the insulator layer is investigated and explained by the variation of the asymptotic frequency of the lower band and the cutoff frequency of the higher band. It is shown that the frequency range of high reflection can be chosen by varying the thickness and the dielectric constant of the insulator layer. The proposed mirror has advantages of easy fabrication for its compact structure, and of frequency range selection. Thus it may be applied to devices such as a beam splitter, a filter, and a cavity for SPPs in photonic integrated circuits.

*yesican@kaist.ac.kr

†cskee@gist.ac.kr

[1] W. L. Barnes, A. Dereux, and T. W. Ebbesen, Nature (London) **424**, 824 (2003).

[2] E. N. Economou, Phys. Rev. **182**, 539 (1969).

[3] C. Davis and T. Tamir, J. Appl. Phys. **37**, 461 (1966).

[4] X. Wang and K. Kempa, Phys. Rev. B **75**, 245426 (2007).

[5] A. R. Zakharian, J. V. Moloney, and M. Mansuripur, Opt. Express **15**, 183 (2007).

[6] Şükrü Ekin Kocabaş, G. Veronis, D. A. B. Miller, and S. Fan, Phys. Rev. B **79**, 035120 (2009).

[7] Y. Kurokawa and H. T. Miyazaki, Phys. Rev. B **75**, 035411 (2007).

[8] M. Kuttge, W. Cai, F. J. García de Abajo, and A. Polman, Phys. Rev. B **80**, 033409 (2009).

[9] B. Prade, J. Y. Vinet, and A. Mysyrowicz, Phys. Rev. B **44**, 13556 (1991).

[10] D.-K. Qing and G. Chen, Phys. Rev. B **71**, 153107 (2005).

[11] K. Y. Kim, Y. K. Cho, H.-S. Tae, and J.-H. Lee, Opt. Express **14**, 320 (2006).

[12] J. A. Dionne, L. A. Sweatlock, H. A. Atwater, and A. Polman, Phys. Rev. B **73**, 035407 (2006).

[13] G. Veronis and S. Fan, Appl. Phys. Lett. **87**, 131102 (2005).

[14] X.-S. Lin and X.-G. Huang, Opt. Lett. **33**, 2874 (2008).

[15] Q. Zhang, X.-G. Huang, X.-S. Lin, J. Tao, and X.-P. Jin, Opt. Express **17**, 7549 (2009).

[16] H. Shin and S. Fan, Phys. Rev. Lett. **96**, 073907 (2006).

[17] M. T. Hill *et al.*, Opt. Express **17**, 11107 (2009).

[18] A. Hossieni and Y. Massoud, Opt. Express **14**, 11318 (2006).

[19] J. Park, H. Kim, and B. Lee, Opt. Express **16**, 413 (2008).

[20] J. Q. Liu, L.-L. Wang, M.-D. He, W.-Q. Huang, D. Wang, B. S. Zou, and S. Wen, Opt. Express **16**, 4888 (2008).

[21] N. García and M. Bai, Opt. Express **14**, 10028 (2006).

[22] P. B. Johnson and R. W. Christy, Phys. Rev. B **6**, 4370 (1972).

[23] MEEP FDTD package [http://jdj.mit.edu/meep].

[24] A. Taflove and S. C. Hagness, *Computational Electrodynamics: The Finite-Difference Time-Domain Method* (Artech House, Norwood, 2005).

[25] T. Uno, Y. He, and S. Adachi, IEEE Microwave Guided Wave Lett. **7**, 264 (1997).

[26] G.-X. Fan and Q. H. Liu, IEEE Antennas Wireless Propag. Lett. (2003).